AGU
ADVANCING EARTH AND SPACE SCIENCES

# Geophysical Research Letters®

**Key Points:**

- Standing waves in rivers indicate unique hydraulic conditions that allow depth and velocity to be inferred from the spacing of the waves
- Critical flow theory can be used to calculate discharge based on measurements of wavelength and width made using readily available images
- Discharges estimated via the critical flow approach for 82 images agreed closely with discharges recorded at gaging stations ($R^2 = 0.98$)

**Author Contributions:**

**Conceptualization:** Carl J. Legleiter, Gordon Grant, Becky Fasth, Laura Hempel
**Data curation:** Carl J. Legleiter, Inhyeok Bae, Becky Fasth
**Formal analysis:** Carl J. Legleiter, Inhyeok Bae, Becky Fasth, Elowyn Yager, Daniel C. White
**Funding acquisition:** Elowyn Yager, Laura Hempel

# Remote Sensing of River Discharge Based on Critical Flow Theory

Carl J. Legleiter[1] , Gordon Grant[2] , Inhyeok Bae[3] , Becky Fasth[4] , Elowyn Yager[3] , Daniel C. White[5] , Laura Hempel[6], Merritt E. Harlan[7] , Christina Leonard[8], and Robert Dudley[9]

[1]U.S. Geological Survey, Observing Systems Division, Golden, CO, USA, [2]U.S.D.A. Forest Service, Pacific Northwest Research Station, Corvallis, OR, USA, [3]Center for Ecohydraulics Research, University of Idaho, Boise, ID, USA, [4]College of Earth, Ocean, and Atmospheric Sciences, Oregon State University, Corvallis, OR, USA, [5]Department of Civil and Environmental Engineering, Colorado State University, Fort Collins, CO, USA, [6]U.S. Geological Survey, Office of Science Quality and Integrity, Pueblo, CO, USA, [7]U.S. Geological Survey, Water Resources Mission Area, Lakewood, CO, USA, [8]Water Resources Division, National Park Service, Fort Collins, CO, USA, [9]U.S. Geological Survey, New England Water Science Center, Pembroke, NH, USA

**Abstract** Critical flow theory provides a physical foundation for inferring discharge from measurements of wavelength and channel width made from images. In rivers with hydraulically steep local slopes greater than ~0.01, flow velocities are high and the Froude number $Fr$ (ratio of inertial to gravitational forces) can approach 1.0 (critical flow) or greater. Under these conditions, undular hydraulic jumps (UHJ's) can form as standing wave trains at slope transitions or constrictions. The presence of UHJ's indicates that mean $Fr \approx 1$, implying that the velocity and depth of the flow and the spacing of the waves are uniquely related to one another. Discharges estimated from 82 Google Earth images agreed closely with discharges recorded at gaging stations ($R^2 = 0.98$), with a mean bias of 1% ± 11%. This approach could provide reliable discharge information in many fluvial environments where critical flow occurs, which tend to be underrepresented in gage networks.

**Plain Language Summary** In some rivers with relatively steep slopes, regularly spaced standing waves can occur where the channel narrows or steepens, forming rapids. These waves remain stationary because the downstream velocity of the flow is equal and opposite to the upstream velocity of the waves. We refer to this balance as critical flow and under these conditions the depth and velocity of the water and the spacing of the waves are uniquely related to one another. These conditions form the basis of a remote sensing approach to estimating discharge, which is the volume of water flowing along the river per unit time. This study introduces a method for calculating discharge based on measurements of wavelength and channel width that can be made using widely available images. We compared the resulting estimates to independent measurements made using field-based techniques at nearby gaging stations. We found strong agreement between traditional measurements and critical flow-based estimates derived from 82 Google Earth images. This new technique could provide accurate discharge information for rivers where critical flow occurs, many of which are not measured regularly as part of current gage networks.

## 1. Introduction

Reliable information on river discharge $Q$ is essential for numerous water management applications, ranging from ecological flow requirements during periods of drought to flood hazard mitigation in times of excess. Conventional methods for measuring $Q$ involve placing sensors directly into the flow to measure depth $d$ and velocity $v$ at a number of locations across the channel and laterally integrating their product. This type of data collection is central to discharge monitoring programs, with site visits to gaging stations used to establish and maintain rating curves that link $Q$ to continuous, automated measurements of water level (i.e., stage; Rantz, 1982). This field-based approach is labor-intensive, costly, and can be hazardous for equipment and personnel. These limitations are especially pronounced in locations that are difficult to access, which constrains the number and type of rivers that can be gaged. Remote sensing could provide an alternative means of characterizing flow conditions, with significant advantages in terms of efficiency, spatial coverage, and safety (Conaway et al., 2019).

Developing non-contact approaches for measuring discharge has emerged as a primary research objective, to both advance hydrologic science and satisfy operational needs, particularly in ungaged basins (e.g., Birkinshaw

**Investigation:** Carl J. Legleiter, Gordon Grant, Inhyeok Bae, Becky Fasth, Elowyn Yager, Daniel C. White, Laura Hempel, Merritt E. Harlan, Christina Leonard, Robert Dudley
**Methodology:** Carl J. Legleiter, Gordon Grant, Inhyeok Bae, Becky Fasth, Elowyn Yager, Daniel C. White, Laura Hempel, Merritt E. Harlan, Christina Leonard
**Project administration:** Carl J. Legleiter, Elowyn Yager, Laura Hempel
**Resources:** Carl J. Legleiter, Elowyn Yager, Laura Hempel, Merritt E. Harlan, Robert Dudley
**Software:** Carl J. Legleiter, Inhyeok Bae
**Supervision:** Elowyn Yager
**Validation:** Carl J. Legleiter, Inhyeok Bae, Becky Fasth, Elowyn Yager, Daniel C. White
**Visualization:** Carl J. Legleiter, Inhyeok Bae, Becky Fasth
**Writing – original draft:** Carl J. Legleiter
**Writing – review & editing:** Gordon Grant, Inhyeok Bae, Becky Fasth, Elowyn Yager, Daniel C. White, Laura Hempel, Merritt E. Harlan, Christina Leonard, Robert Dudley

et al., 2014; Gleason & Durand, 2020). Over several decades, numerous techniques for remote sensing of flow depth and velocity have matured, but the limitations of these methods restrict the range of river environments where they can be applied. For example, although spectrally based depth retrieval and bathymetric lidar can be highly accurate in shallow, clear-flowing streams (e.g., Legleiter & Harrison, 2019), their performance degrades in deeper, more turbid rivers (e.g., Kwon et al., 2024). Conversely, image velocimetry has proven effective in sediment-laden rivers (Legleiter & Kinzel, 2020) but if the water is clear, the flow often must be seeded with artificial particles (Biggs et al., 2022). More specialized instrumentation could help circumvent these issues, but technologies like ground-penetrating radar, which can be used to infer turbid depths (e.g., Bandini et al., 2023), and thermal image velocimetry, which could obviate the need for seeding (e.g., Schweitzer & Cowen, 2021), are not yet widely available or extensively tested.

In the context of discharge measurement, this situation results in a conundrum: rivers conducive to bathymetric mapping might not be amenable to velocity estimation and vice versa. In addition, many existing methods rely upon field measurements to calibrate a relationship between depth and reflectance (e.g., Legleiter & Harrison, 2019). Similarly, techniques like particle image velocimetry involve computationally intensive algorithms that must be parameterized on a case-by-case basis. Calculating discharge based on image-derived velocity estimates also requires an independent source of information on the cross-sectional area of the channel. Although these approaches are non-contact, they require travel to a site and are often applied only at a reach scale. Obtaining the equipment and software needed to set up and sustain such a monitoring program could be a sizable investment and implementing the associated complex workflows also requires personnel with technical expertise.

Acquiring data from fixed wing aircraft or satellites can provide broader coverage and these platforms have been used to map both depth (e.g., Legleiter & Harrison, 2019) and velocity (Legleiter et al., 2023; Masafu et al., 2023). However, coordinating with flight contractors is challenging and satellite images of sufficient spatial resolution are expensive and subject to clouds and atmospheric effects. Another current thrust in remote sensing of rivers focuses on the Surface Water and Ocean Topography (SWOT) mission, a satellite-based radar designed to provide information on rivers greater than 100 m in width. Several algorithms for inferring discharge from SWOT observations of water surface elevation, width, and slope have been proposed, but these methods require assumptions regarding channel geometry and roughness and are still being refined (Durand et al., 2023).

Despite recent developments in remote sensing, a need for additional methods of inferring discharge from river images persists. Ideally, these approaches would be inexpensive, based upon readily available data, and easy to apply with standard software tools and minimal training. In this study, we introduce a new technique that satisfies these criteria: in rivers where standing waves are present, measurements of their wavelength and the channel width can be used to estimate discharge based on the concept of critical flow. The following sections: (a) summarize the underlying theory, (b) list the characteristics of sites where the method might be applied and describe how to perform measurements, (c) assess the accuracy of the resulting discharge estimates via comparison to gage records and quantify their sensitivity to measurement error, and (d) discuss the implications of our findings.

## 2. Critical Flow Theory

Our remote sensing approach builds upon previous work by Tinkler (1997) and Grant (1997) and is based on the hypothesis that trains of standing waves indicate critical flow conditions. Critical flow occurs when inertial and gravitational forces are balanced, hence the flow velocity is equal and opposite to the velocity (celerity) of an upstream-propagating wave (Henderson, 1966; Kennedy, 1963). As a result, the waves appear to stand still. Critical flow is indicated by a Froude number $Fr$ equal to 1.0, with

$$Fr = \frac{v}{\sqrt{gd}} \tag{1}$$

where $v$ is flow velocity, $d$ is depth, and $g$ is gravitational acceleration.

Critical flow represents a threshold between two energy states: supercritical where $Fr > 1$ and subcritical where $Fr < 1$. This condition also represents the minimum specific energy for a given discharge, as well as the maximum discharge for a given specific energy. Critical flow is thus very "efficient" and might act as an attractor for flow conditions (Grant, 1997). The transition between super- and sub-critical flow is accompanied by an
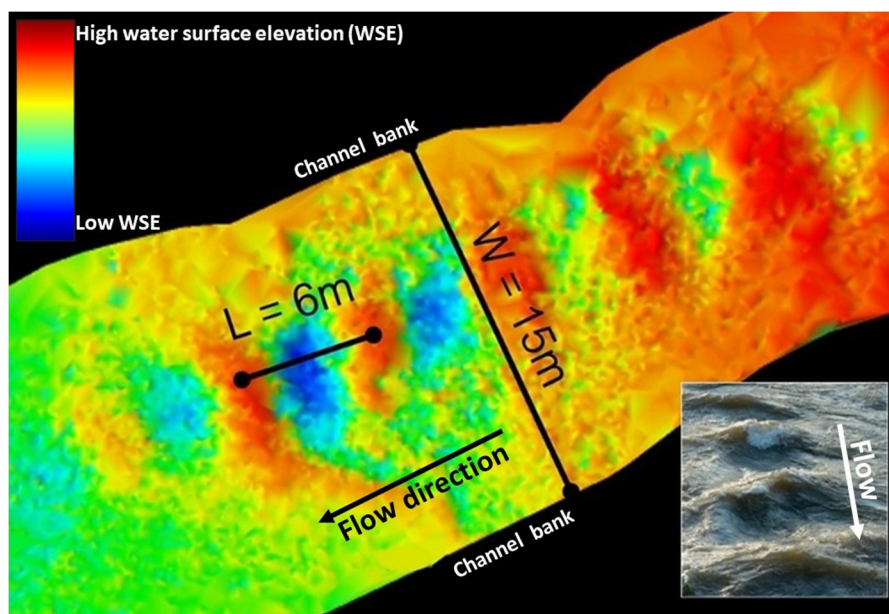
**Figure 1.** Terrestrial laser scan of Clear Creek, Colorado, with well-defined undular hydraulic jumps (UHJ's). Red and blue colors represent relatively high and low water surface elevations, respectively, and the channel banks are masked out and shown in black. The inset photo shows an oblique view of UHJ's on a river in Oregon. Laser scan and photo courtesy of Toby Minear and Gordon Grant, respectively.

energy loss in the form of waves and turbulence. Where this transition is abrupt, as might occur just downstream of a submerged obstruction or sharp slope break, a solitary hydraulic jump will form. Where the forcing occurs more gradually, for example, at flow constrictions or less abrupt changes in gradient, the resulting wave pattern is a train of standing waves termed undular hydraulic jumps (UHJ's, Henderson, 1966).

UHJ's are the foundation of our approach. They typically occur in hydraulically steep rivers with local slopes greater than ~0.01 (Grant, 1997) and are visible as a sequence of multiple regularly spaced peaks and troughs, often spanning a large fraction of the channel width. The peaks might have sharp, rolling, or breaking waves, often creating whitewater. An example is shown in Figure 1, which depicts a terrestrial laser scan with well-defined UHJ's. The wavelength $L$ of these waves can be measured from an image, as can the wetted channel width $w$. Critical flow theory provides a means of estimating $Q$ based solely upon these two measurements. This method was first proposed by Dietterich et al. (2022) as a way to infer the effusion rate of lava, but their results could not be evaluated easily due to a lack of independent techniques for measuring lava depth. Applying this critical flow-based approach to rivers allows us to test the method by comparing discharge estimates to measurements from gaging stations.

Dietterich et al. (2022) provided a thorough treatment of the hydraulics of UHJ's and their relationship to critical flow; we revisit only a few key points herein. Flume experiments (e.g., Chanson, 1995) and field measurements (Grant, 1997) have confirmed that within these wave trains $Fr \approx 1.0$, although flow oscillates between supercritical in troughs and subcritical in crests. Grant (1997) postulated that this phenomenon requires a mobile bed, but numerous flume studies have demonstrated that UHJ's can form where the bed is fixed or stationary (Chanson, 1995; Chanson & Montes, 1995; Dietterich et al., 2022; Henderson, 1966). In addition, Tinkler (1997) documented UHJ's in a river with an immobile bed. Kennedy (1963) showed that the stationary jump wavelength $L$ scales with flow velocity:

$$L = 2\pi \frac{v^2}{g} \qquad (2)$$

This expression can be rearranged to relate velocity to wavelength:

$$v = \sqrt{\frac{Lg}{2\pi}} \tag{3}$$

Assuming that $Fr \approx 1.0$ and that the downstream flow velocity is equal to the wave celerity (Kennedy, 1963), we use Equation 1 to then calculate depth:

$$d = \frac{v^2}{g} \tag{4}$$

Combining Equations 3 and 4 with a measurement of width $w$ allows discharge to be estimated from $L$:

$$Q = vdw = \frac{g^{1/2}}{(2\pi)^{3/2}} L^{3/2} w \tag{5}$$

We hypothesize that this expression, along with basic measurements of $L$ and $w$ from readily available image data, are all that is required to infer river discharge when clearly defined UHJ's are present.

## 3. Materials and Methods

For this proof-of-concept investigation, we selected sites for evaluating the critical flow approach based upon several criteria. First, to assess accuracy via comparison to independent measurements of discharge, we only considered locations within a few km of U.S. Geological Survey (USGS) (2025) gages, with no intervening tributary inputs or diversions between the site and the gage. Some sites were upstream of the associated gaging station whereas others were downstream. Second, the area around the UHJ's should be free of obstructions such as boulders, stationary hydraulic jumps that are an expression of localized supercritical (as opposed to critical) flow, or oblique waves propagating from the channel banks (e.g., Kieffer, 1985). In addition, the UHJ's should span a large fraction of the width, from approximately 40% up to 100% of the channel surface area. Third, we used our experience and the communal knowledge of recreationalists to restrict our search to reaches with well-known rapids that exhibit UHJ's. We identified additional candidates by filtering an OpenStreetMap (2024) "rapids" layer to reaches within 500 m of USGS gages. For each prospective site, we used free Google Earth Pro software (Google, 2024) to examine images of the reach and assess suitability for critical flow analysis. Ideal sites featured well-defined UHJ's with clearly visible wave peaks and troughs, typically expressed as whitewater. To avoid ambiguities in width measurement, we excluded images where the wetted channel width changed abruptly near the UHJ's.

This selection process led to 24 distinct rapids associated with the 15 gaging stations shown in Figure S1 in Supporting Information S1; up to four rapids were associated with a single gage. These sites are mainly in the western U.S., where rivers with relatively steep slopes and minimal vegetation are common. For many of the selected rapids, multiple image dates were deemed amenable to analysis, with a median of 3 images per rapid and as many as 10 (refer to Figure S2 in Supporting Information S1). Site selection was completed before any discharge calculations were performed and in total our data set consisted of 82 river images, with one measured UHJ per image. While this inventory was not systematically acquired to serve as a representative sample, these images provide a sufficient number of observations to assess the feasibility of our approach. All the data used in this study are available from Legleiter et al. (2024).

For each date at each rapid, we used tools within Google Earth Pro to measure the two variables required to estimate $Q$ via Equation 5: $L$ and $w$. Based on visual inspection, we measured two separate, consecutive wavelengths immediately adjacent to one another where the UHJ was most clearly expressed as variations in brightness. Wavelengths were measured from one wave crest to the next, with the crests often appearing as the brightest part of the river due to the presence of white water or foam where the waves break. Channel width was measured by creating another line oriented perpendicular to the wavelength measurements and located at the midpoint between them. In a few cases, this line was not perpendicular to the banks. To minimize uncertainty associated with variations in width, we made these measurements where width remained relatively uniform along the length of the UHJ's. Examples of these features are provided in Figure 2. While this process involved a degree of subjectivity, all measurements were made by a single operator to avoid user-dependent bias and ensure that a
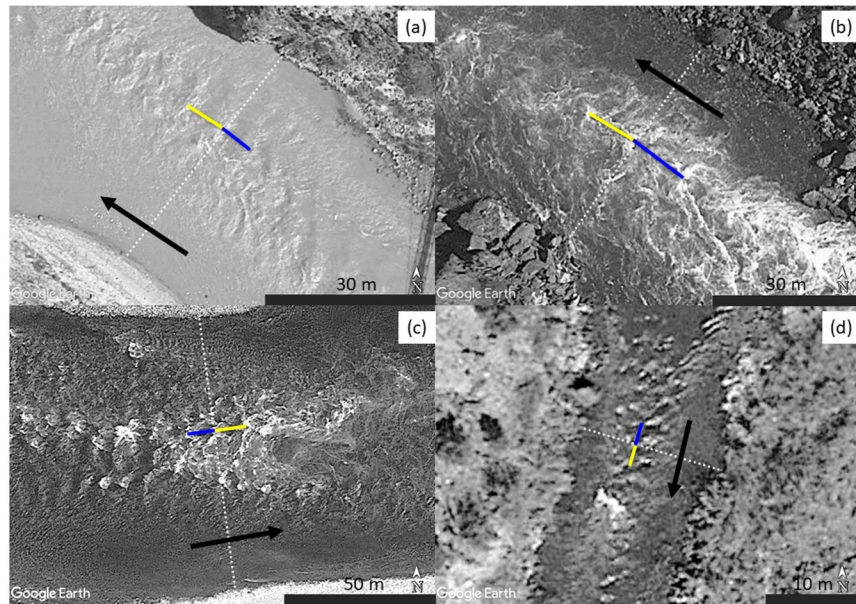
**Figure 2.** Example rapids and measurements of width (white dotted lines) and two sequential wavelengths (blue and yellow lines) made in Google Earth. Flow direction indicated by black arrows. (a) Bright Angel Rapid, Colorado River, 7 April 2022. (b) Horn Rapid, Colorado River, 26 June 2017. (c) Lewis Rapid, Snake River, 5 August 2014. (d) Hondo Rapid, Rio Grande, 2 March 2021.

consistent methodology was applied. Text S1 in Supporting Information S1 provides further detail on the measurement procedure and all 82 images with measurement lines are included in Data Set S1.

We also digitized another type of feature: a shadow cast by a vertical object such as a utility pole, tree, or building. We used the orientation of the shadow to infer when the image was acquired. The "sundial" method described in Text S2 in Supporting Information S1 involves using the latitude, longitude, and image date to calculate solar azimuths at various times throughout the day following Reda and Andreas (2004); the time when the sun was positioned so as to cast the observed shadow is taken to be the image acquisition time. This information enabled us to use "instantaneous" gage records with a 15-min sampling interval, which was important because diurnal fluctuations in discharge can be pronounced below hydropower dams. This refinement allowed us to include 24 images of four separate rapids along the Colorado River in the Grand Canyon, where flows are influenced by the operation of Glen Canyon Dam (Hazel et al., 2006).

We developed code to automate the following tasks (Legleiter, 2024): (a) import data from Google Earth; (b) organize by rapid and image date; (c) extract measurements of $L$, $w$, and shadow orientation; (d) infer image acquisition time via the sundial method; (e) perform two discharge calculations via Equation 5, one for each wavelength measurement, and take their average to obtain the final discharge estimate; and (f) retrieve the discharge measured at the corresponding gaging station. Overall, the 82 gage discharges varied from 3.88 to 1,135 $m^3$/s with a median of 183 $m^3$/s. Measured widths varied from 12.1 to 160 m with a median of 46.7 m and wavelengths ranged from 1.23 to 15.8 m with a median of 7.08 m (refer to Figure S3 in Supporting Information S1).

As a test of the critical flow-based approach, we compared our $Q$ estimates to gaged discharges. This accuracy assessment involved using the image-derived $Q$ estimate to calculate the percent error as

$$\varepsilon = \frac{Q_c - Q_g}{Q_g} \times 100,$$

(6)

where $Q_c$ refers to the critical flow-based discharge and $Q_g$ to that measured at the gage. We also performed an observed versus predicted regression to quantify the strength of the relationship between $Q_c$ and $Q_g$.
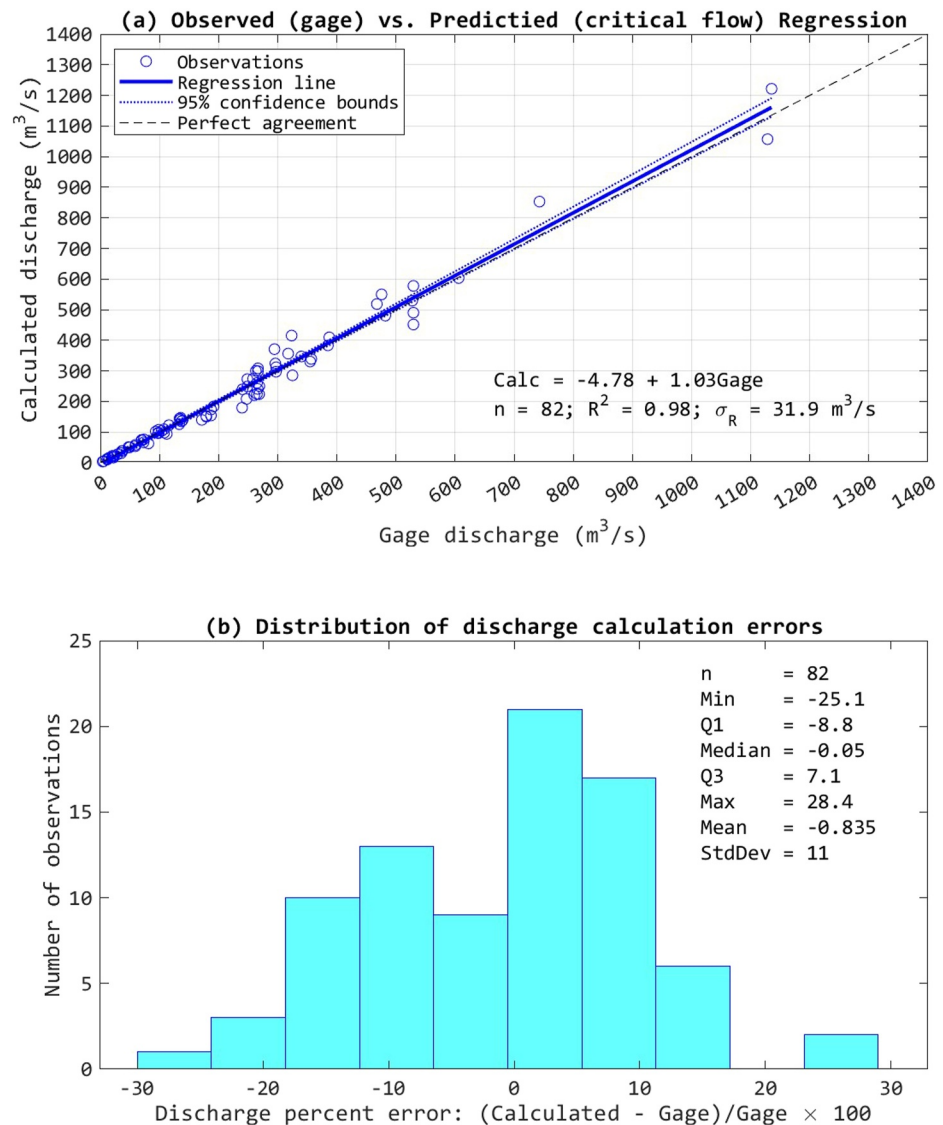
**Figure 3.** (a) Observed versus predicted regression comparing discharges recorded at gaging stations to those calculated using Equation 5. The symbol $\sigma_r$ refers to the standard deviation of residuals from the regression line. (b) Histogram and summary statistics for discharge estimation errors.

We conducted a sensitivity analysis to quantify how estimates of $Q$ might be affected by errors in the measurement of $L$ and $w$. To quantify the uncertainty in $Q$ estimates that could result from a given level of measurement error, we first used the median $L$ and $w$ from our data set to establish a baseline $Q$ via Equation 5. We then considered a scenario where measurement errors in $L$ and $w$ each follow a zero-mean normal distribution and are independent of one another. The standard deviation of each distribution was set as a percentage (0%–25%) of the 25th, 50th, and 75th percentiles of the $L$ and $w$ measurements made for this study. We then generated 1,000 random samples from each of these six distributions. For each percentile, $Q$ estimates were calculated for cases where (a) only $L$ varied, (b) only $w$ varied, or (c) both $L$ and $w$ varied. The uncertainty associated with measurement errors was summarized in terms of the standard deviation of $Q$ estimation errors. Additional detail on this analysis is in Text S3 of Supporting Information S1.

## 4. Results

Our results are summarized in Figure 3, which shows strong agreement between observed and predicted $Q$ across three orders of magnitude. The $R^2$ of 0.98 indicates nearly perfect correlation between $Q_c$ and $Q_g$ (Figure 3a), with

a slope near 1 and an intercept near 0 implying that estimates were unbiased (Pineiro et al., 2008). The distribution of errors shown in Figure 3b provides further evidence that image-derived discharges were not biased; the mean and median of the estimated discharges were within 1% of the measured discharges. These estimates were also relatively precise, with a standard deviation and inter-quartile range of 11% and 16%, respectively. The distribution was approximately symmetric and even at the extremes, $Q_c$ did not differ from $Q_g$ by more than 28.4%. In addition, $\varepsilon$ was not significantly correlated with $Q_g$ (correlation coefficient $\rho = 0.137$, $p = 0.22$; Figure S4 in Supporting Information S1), implying that the method performed well across the full range of discharges.

However, sensitivity analyses indicated that errors in $L$ and $w$ measurement could impact discharge estimates. For example, inspection of Equation 5 indicates that an $\epsilon$ error in only $L$, only $w$, or both $L$ and $w$ would lead to uncertainties in $Q$ of $(1 + \epsilon)^{3/2}$, $\epsilon$, or $(1 + \epsilon)^{2.5}$, respectively. If the measurement errors in $L$ and $w$ are assumed to be normally distributed and independent of one another, the standard deviation of $Q$ estimation errors varies as $1.5\epsilon$ if only $L$ varies, $\epsilon$ if only $w$ varies, or $1.8\epsilon$ if both $L$ and $w$ vary. Repeating these calculations based on the 25th, 50th, and 75th percentiles of $L$ and $w$ indicates that streams of all sizes are subject to the same level of uncertainty (refer to Figure S5 in Supporting Information S1). As an example, for the median values of $L$ and $w$ from this study, a 5% measurement error could translate into a 9% error in $Q$. This finding implies that our measurements, which led to discharge estimation errors with a standard deviation of 11% (Figure 3), were probably accurate to within 5%.

## 5. Discussion

These results indicate that remote sensing of discharge based on critical flow theory is not only feasible but potentially highly accurate. The approach compares favorably to other methods of measuring discharge, whether by conventional field methods or non-contact techniques. For example, McMillan et al. (2012) concluded that calculating discharge from a rating curve is associated with an uncertainty of at least 10%, on the same order as the 11% standard deviation of $\varepsilon$ reported herein. While gage records are often treated as the "gold standard," recent studies have shown that the errors inherent to rating curve-based estimates vary widely among sites (Coxon et al., 2017) and depend on the method used to quantify the error (Kiang et al., 2018). Similarly, although the algorithms developed to support the SWOT mission might be considered the state of the art in remote sensing of discharge, typical uncertainties are on the order of 30% (Durand et al., 2023). For the limited sample used in this initial study, even the largest errors were less than 30%, implying that the critical flow-based approach, where applicable, could yield discharge information as reliable as that provided by existing techniques.

Although our initial findings are encouraging, we also acknowledge that the critical flow-based approach is limited in several respects. Most importantly, our methodology can only be applied where and when well-defined UHJ's are clearly visible in an image; the range of applicability does not encompass all rivers. The flow conditions under which these features form are most often observed in rivers with slopes greater than 0.01, or in association with channel constrictions. UHJ's are thus most likely to occur in steep mountain streams and canyon rivers, whereas lowland rivers with gentle gradients are not amenable to this approach. However, a slope in excess of 0.01 is not an essential criterion and UHJ's can be present within rapids in reaches with overall gradients less than 0.01. For example, the average slope of the Colorado River through the Grand Canyon is only 0.0015 but large UHJ's are found in rapids with local slopes ranging from 0.02 to 0.03 (Magirl et al., 2009). The USGS National Hydrographic Dataset (NHD) (Moore et al., 2019) provides some insight as to how common UHJ's might be. The distribution of slopes for over 2.6 million NHD stream reaches is summarized in Figure S6 in Supporting Information S1, which shows that although the majority of reaches have slopes that are likely too gentle for critical flow to occur, over 40% of reaches had slopes >0.01, which is an approximate, conservative threshold for the occurrence of UHJ's. Many of these reaches occur in small headwater streams that might not be conducive to remote sensing due to limited spatial resolution and/or overhanging vegetation, but our method might have a broader range of applicability than anticipated.

Another limitation of the critical flow approach is that several sources of error could reduce the accuracy and precision of discharge estimates; potential users of this technique are cautioned not to assume, or even expect, that agreement between calculated discharges and gage measurements will be as strong as that reported herein. This study merely demonstrated that some UHJs include waves with dimensions that, when combined with measurements of channel width, accurately reproduce discharges recorded at gaging stations. Our current measurement process relies upon visual inspection of images and manual digitization of wavelengths and channel

widths. These inputs are thus subjective and susceptible to both systematic and random uncertainties, such as operator bias and measurement error. The choice of which waves to measure, in particular, involves expert judgment; further work could help to develop a wave selection process that is as repeatable as possible. In addition, the size of the features of interest relative to the spatial resolution of the image could affect the amount of error, which will likely be greater when the image pixel size is a large fraction of the wavelength and width in the channel of interest. Another source of uncertainty is the proportion of the channel width occupied by UHJ's. The complex, disorganized flow fields in rapids could also lead to spatial variation in the validity of the assumption that $Fr \approx 1$.

Despite these potential shortcomings, techniques based on critical flow theory could facilitate operational streamgaging and thus contribute to the mission of water monitoring agencies. For example, we extracted slopes at 8,453 active streamgages in the USGS National Water Information System from the NHD and found that 12% had reach slopes >0.01 (refer to Figure S8 in Supporting Information S1). This initial census suggests that, at a minimum, a non-contact approach based on critical flow theory could complement current streamgaging operations for a non-trivial fraction of the USGS hydrologic monitoring network that is currently underrepresented.

This initial investigation provided a proof of concept, but future research could yield insight regarding the applicability and limitations of critical flow-based techniques for remote sensing of discharge. For example, a more systematic inventory of stream reaches would constrain the range of slopes where UHJ's occur, provide guidance for site selection, and help to define what proportion of rivers might be amenable to our approach. Because rivers with whitewater are visually distinct, deep learning algorithms might be helpful for extracting candidate images from archives of remotely sensed data (e.g., Hedger & Gosselin, 2023). Another important topic to address is the subjectivity of the initial wave selection and subsequent wavelength and width measurements that comprise the core of the workflow. A more thorough sensitivity analysis focused on these inputs could lead to an error budget for critical flow-based discharge estimates. Such an inquiry could also help to establish guidelines for making these measurements as reproducibly as possible. Although the basic theory summarized in Section 2 provides a solid basis for our approach, several assumptions are involved, most notably that the flow is deep relative to the wavelength of the UHJ's, with $d > 0.5L$. Revisiting these assumptions could yield additional insight regarding the underlying physical processes giving rise to the observed relations between $L$, $v$, $d$, and $Q$ and could point toward possible refinements in cases where, for example, $d < 0.5L$ and the deep water assumption (Kennedy, 1963) might not hold. Such an analysis could be based upon existing flume data sets such as those cited by Dietterich et al. (2022). Finally, developing software tools for implementing a more automated workflow could help to provide consistent results and make this promising new technique accessible to a broader community.

The framework introduced in this study offers a number of advantages relative to other non-contact methods of measuring discharge. For example, whereas mapping both velocity and depth simultaneously with a single sensor might not be possible due to constraints on particle image velocimetry and spectrally based depth retrieval, critical flow theory provides a solid foundation for calculating both $v$ and $d$, and thus $Q$, from a single remotely sensed data set. Moreover, images suitable for this type of analysis are already available through public servers, with no new data collection required. Similarly, rather than specialized processing software and computationally demanding algorithms, the critical flow approach requires only simple measurements of wavelength and width that can be made via intuitive user interfaces. Because both suitable images and measurement tools are packaged within free software and no further investment in instrumentation or travel to field sites is needed, this approach could also be highly cost-effective. Risks to equipment and personnel could be eliminated.

## Data Availability Statement

The data used in this study are available through a data release (Legleiter et al., 2024). Code developed to analyze these data is provided in a separate software release (Legleiter, 2024).

## References

Bandini, F., Kooij, L., Mortensen, B. K., Caspersen, M. B., Thomsen, L. G., Olesen, D., & Bauer-Gottwein, P. (2023). Mapping inland water bathymetry with ground penetrating radar (GPR) on board unmanned aerial systems (UASs). *Journal of Hydrology*, *616*, 128789. https://doi.org/10.1016/j.jhydrol.2022.128789

Biggs, H. J., Smith, B., Detert, M., & Sutton, H. (2022). Surface image velocimetry: Aerial tracer particle distribution system and techniques for reducing environmental noise with coloured tracer particles. *River Research and Applications*, *38*(6), 1192–1198. https://doi.org/10.1002/rra.3973

Birkinshaw, S. J., Moore, P., Kilsby, C. G., O'Donnell, G. M., Hardy, A. J., & Berry, P. A. M. (2014). Daily discharge estimation at ungauged river sites using remote sensing. *Hydrological Processes*, *28*(3), 1043–1054. https://doi.org/10.1002/hyp.9647

Chanson, H. (1995). *Flow characteristics of undular hydraulic jumps. Comparison with near-critical flows (tech. Rep. No. 45)*. Department of Civil Engineering, The University of Queensland.

Chanson, H., & Montes, J. S. (1995). Characteristics of undular hydraulic jumps: Experimental apparatus and flow patterns. *Journal of Hydraulic Engineering*, *121*(2), 129–144. https://doi.org/10.1061/(asce)0733-9429(1995)121:2(129)

Conaway, J., Eggleston, J., Legleiter, C., Jones, J., Kinzel, P., & Fulton, J. (2019). Remote sensing of river flow in Alaska—New technology to improve safety and expand coverage of USGS streamgaging. *U.S. Geological Survey Fact Sheet*, *2019*(3024), 4. https://doi.org/10.3133/fs20193024

Coxon, G., Freer, J., Westerberg, I. K., Wagener, T., Woods, R., & Smith, P. J. (2017). A novel framework for discharge uncertainty quantification applied to 500 UK gauging stations. *Water Resources Research*, *51*(7), 5531–5546. https://doi.org/10.1002/2014wr016532

Dietterich, H. R., Grant, G. E., Fasth, B., Major, J. J., & Cashman, K. V. (2022). Can lava flow like water? Assessing applications of critical flow theory to channelized basaltic lava flows. *Journal of Geophysical Research: Earth Surface*, *127*(9), e2022JF006666. https://doi.org/10.1029/2022jf006666

Durand, M., Gleason, C. J., Pavelsky, T. M., de Moraes Frasson, R., Turmon, M., David, C. H., et al. (2023). A framework for estimating global river discharge from the surface water and ocean topography satellite mission. *Water Resources Research*, *59*(4), e2021WR031614. https://doi.org/10.1029/2021wr031614

Gleason, C. J., & Durand, M. T. (2020). Remote sensing of River Discharge: A review and a framing for the discipline. *Remote Sensing*, *12*(7), 1107. https://doi.org/10.3390/rs12071107

Google. (2024). Earth versions - Google Earth. Retrieved from https://www.google.com/earth/about/versions/

Grant, G. E. (1997). Critical flow constrains flow hydraulics in mobile-bed streams: A new hypothesis. *Water Resources Research*, *33*(2), 349–358. https://doi.org/10.1029/96wr03134

Hazel, J. E. Jr., Topping, D. J., Schmidt, J. C., Kaplinski, M., Hazel, J. E., Topping, D. J., & Kaplinski, M. (2006). Influence of a dam on fine-sediment storage in a canyon river. *Journal of Geophysical Research*, *111*(1), 1–16. https://doi.org/10.1029/2004jf000193

Hedger, R. D., & Gosselin, M.-P. (2023). Automated fluvial hydromorphology mapping from airborne remote sensing. *River Research and Applications*, *39*(9), 1889–1901. https://doi.org/10.1002/rra.4186

Henderson, F. (1966). Open Channel flow.

Kennedy, J. F. (1963). The mechanics of dunes and antidunes in erodible-bed channels. *Journal of Fluid Mechanics*, *16*(4), 521–544. https://doi.org/10.1017/s0022112063000975

Kiang, J. E., Gazoorian, C., McMillan, H., Coxon, G., Le Coz, J., Westerberg, I. K., et al. (2018). A comparison of methods for streamflow uncertainty estimation. *Water Resources Research*, *54*(10), 7149–7176. https://doi.org/10.1029/2018wr022708

Kieffer, S. W. (1985). The 1983 hydraulic jump in crystal rapid: Implications for river-running and geomorphic evolution in the Grand canyon. *The Journal of Geology*, *93*(4), 385–406. https://doi.org/10.1086/628962

Kwon, S., Passalacqua, P., Soloy, A., Jensen, D., & Simard, M. (2024). Depth mapping in turbid and deep waters using AVIRIS-NG imagery: A study in wax lake delta, Louisiana, USA. *Water Resources Research*, *60*(11), e2023WR036875. https://doi.org/10.1029/2023wr036875

Legleiter, C. J. (2024). Critflowq (ver. 1.0.0, December, 2024) [Software]. *U.S. Geological Survey software release*. https://doi.org/10.5066/P1OIDFH4

Legleiter, C. J., Bae, I., Fasth, B., Grant, G., Yager, E., White, D., et al. (2024). Image-based measurements and gage records used to test a method for inferring river discharge from remotely sensed data based on critical flow theory [Dataset]. *U.S. Geological Survey Data Release*. https://doi.org/10.5066/P1Q3CALH

Legleiter, C. J., & Harrison, L. R. (2019). Remote sensing of River bathymetry: Evaluating a range of sensors, platforms, and algorithms on the upper Sacramento River, California, USA. *Water Resources Research*, *55*(3), 2142–2169. https://doi.org/10.1029/2018wr023586

Legleiter, C. J., & Kinzel, P. J. (2020). Inferring surface flow velocities in sediment-laden Alaskan rivers from optical image sequences acquired from a helicopter. *Remote Sensing*, *12*(8), 1282. https://doi.org/10.3390/rs12081282

Legleiter, C. J., Kinzel, P. J., Laker, M., & Conaway, J. S. (2023). Moving aircraft river velocimetry (MARV): Framework and proof-of-concept on the Tanana River. *Water Resources Research*, *59*(2), e2022WR033822. https://doi.org/10.1029/2022wr033822

Magirl, C. S., Gartner, J. W., Smart, G. M., & Webb, R. H. (2009). Water velocity and the nature of critical flow in large rapids on the Colorado River, Utah. *Water Resources Research*, *45*, W05427. https://doi.org/10.1029/2009WR007731

Masafu, C., Williams, R., & Hurst, M. D. (2023). Satellite video remote sensing for estimation of river discharge. *Geophysical Research Letters*, *50*(24), e2023GL105839. https://doi.org/10.1029/2023gl105839

McMillan, H., Krueger, T., & Freer, J. (2012). Benchmarking observational uncertainties for hydrology: Rainfall, river discharge and water quality. *Hydrological Processes*, *26*(26), 4078–4111. https://doi.org/10.1002/hyp.9384

Moore, R. B., McKay, L. D., Rea, A. H., Bondelid, T. R., Price, C. V., Dewald, T. G., & Johnston, C. M. (2019). *User's guide for the national hydrography dataset plus (NHDPlus) high resolution (Tech. Rep. No. 2019-1096)*. U.S. Geological Survey.

OpenStreetMap. (2024). OpenStreetMap. Retrieved from https://openstreetmap.org

Pineiro, G., Perelman, S., Guerschman, J. P., Paruelo, J. M., Pi, G., Perelman, S., & Guerschman, J. P. (2008). How to evaluate models: Observed vs. predicted or predicted vs. observed? *Ecological Modelling*, *216*(3–4), 316–322. https://doi.org/10.1016/j.ecolmodel.2008.05.006

Rantz, S. (1982). Measurement and computation of streamflow: Volume 1. Measurement of stage and discharge (Vol. *2175*).

Reda, I., & Andreas, A. (2004). Solar position algorithm for solar radiation applications. *Solar Energy*, *76*(5), 577–589. https://doi.org/10.1016/j.solener.2003.12.003

Schweitzer, S. A., & Cowen, E. A. (2021). Instantaneous river-wide water surface velocity field measurements at centimeter scales using infrared quantitative image velocimetry. *Water Resources Research*, *57*(8), e2020WR029279. https://doi.org/10.1029/2020wr029279

Tinkler, K. J. (1997). Critical flow in rockbed streams with estimated values for Manning's *n*. *Geomorphology*, *20*(1), 147–164. https://doi.org/10.1016/s0169-555x(97)00011-1

U.S. Geological Survey. (2025). *USGS water data for the Nation*. U.S. Geological Survey National Water Information System database. https://doi.org/10.5066/F7P55KJN